Biochemistry

 Volume 38, Number 3 January 19, 1999

Accelerated Publications

Solution Structure of the Sodium Channel Inactivation Gate[†,‡]

Carol A. Rohl,[§] Faye A. Boeckman,[||] Carl Baker,[||] Todd Scheuer,[||] William A. Catterall,[||] and Rachel E. Klevit*[,§]

Department of Biochemistry, University of Washington, Seattle, Washington 98195, and Department of Pharmacology, University of Washington, Seattle, Washington 98195

Received September 30, 1998; Revised Manuscript Received November 17, 1998

ABSTRACT: The sodium channel initiates action potentials by opening in response to membrane depolarization. Fast channel inactivation, which is required for proper physiological function, is mediated by a cytoplasmic loop proposed to occlude the ion pore via a hinged lid mechanism with the triad IFM serving as a hydrophobic "latch". The NMR solution structure of the isolated inactivation gate reveals a stably folded core comprised of an α-helix capped by an N-terminal turn, supporting a model in which the tightly folded core containing the latch motif pivots on a more flexible hinge region to occlude the pore during inactivation. The structure, in combination with substituted cysteine mutagenesis experiments, indicates that the IFM triad and adjacent Thr are essential components of the latch and suggests differing roles for the residues of the IFMT motif in fast inactivation.

Voltage-gated sodium channels are responsible for initiating and propagating action potentials in a variety of excitable cells (*1*−*4*). In response to membrane depolarization, sodium channels open, allowing an influx of sodium through an ion-selective pore. During maintained depolarization, the channels convert to an inactivated, nonconducting state on a millisecond time scale, and repolarization of the membrane is required for recovery from inactivation. An intracellular gate that is sensitive to proteases is hypothesized to occlude the pore during inactivation (*5*). The physiological importance of the inactivation process is underscored by the fact that it is a target for paralytic neurotoxins (*1*) and mutations that cause periodic paralysis of skeletal muscle and long QT syndrome in the heart (*3*, *6*). In addition, inactivation is the target of neurotransmitter modulation of sodium current via the protein kinase C (PKC)[1] pathway; activation of muscarinic acetylcholine receptors slows sodium channel inactivation and reduces peak sodium currents in a PKC-dependent manner (*7*).

The sodium channel from rat brain is a heterotrimeric protein with an $\alpha\beta_1\beta_2$ composition, but expression of the α-subunit is sufficient to provide voltage-sensitive sodium gating in vitro (*1*, *2*). The 260 kDa α-subunit contains four homologous transmembrane domains connected by cytoplasmic linkers. The intracellular linker between domains III and IV has been identified as the inactivation domain: antibodies directed against the III−IV linker completely block fast inactivation (*8*, *9*); inactivation is absent in channels in which

[†] This work was supported by NIH Grant RO1 DK35187 to R.E.K. and NIH Grant RO1 NS15751 to W.A.C. C.A.R. is a fellow of the Cancer Research Fund of the Damon Runyon-Walter Winchell Foundation (DRG-1405). F.A.B. was supported by an NRSA postdoctoral fellowship (F32 NS10521).

[‡] Coordinates for the final ensemble of 10 structures have been deposited in the Brookhaven Protein Data Bank under file name 1byy.

* To whom correspondence should be addressed. E-mail: klevit@u.washington.edu.

[§] Department of Biochemistry, University of Washington.

[||] Department of Pharmacology, University of Washington.

[1] Abbreviations: PKC, protein kinase C; NMR, nuclear magnetic resonance; MALDI, matrix-assisted laser desorption ionization; hNOE, heteronuclear nuclear Overhauser enhancement; NOE, nuclear Overhauser enhancement; MTSET, [2-(trimethylammonium)ethyl]methanethiosulfonate bromide; MTS, methanethiosulfonate.

10.1021/bi9823380 CCC: $18.00
Published on Web 12/23/1998

this linker is clipped and domain IV is expressed independently of domains I−III (*10*); and deletions or mutations in the III−IV linker slow or destroy inactivation (*11*, *12*). A hydrophobic triad of amino acids, IFM (residues 1488−1490), has been identified as a motif critical for inactivation. Substitution of these three residues with glutamine completely blocks inactivation (*13*), and inactivation can be restored by the addition of short peptides containing the IFM motif (*14*, *15*). Thiol modification experiments indicate that the III−IV linker undergoes a conformational change associated with inactivation that renders the phenylalanine in the IFM motif inaccessible, leading to the proposal that the III−IV linker functions as a hinged lid with the IFM motif serving as a hydrophobic latch that occludes the ion pore (*16*). To investigate the mechanism by which the III−IV linker mediates fast inactivation, the NMR solution structure of a protein fragment corresponding to the III−IV linker has been determined using standard homo- and heteronuclear methods.

EXPERIMENTAL PROCEDURES

Sample Preparation. The DNA sequence encoding residues 1474−1526 of the rat brain sodium channel α-subunit was inserted into pGEX (Pharmacia). The resulting glutathione *S*-transferase fusion protein was expressed in BL26 cells in either LB media or minimal media containing 1 g/L $^{15}NH_4Cl$ and 2 g/L [^{13}C]glucose or 4 g/L [^{12}C]glucose. The GST fusion was purified on glutathione resin according to the manufacturer's protocol, cleaved with thrombin (Novagen), and purified by reverse phase HPLC on a C18 column (Vydac) in water/acetonitrile gradients containing 0.1% trifluoroacetic acid. The purity was greater than 95% as assessed by Coomassie-stained SDS gels. The molecular mass was confirmed by MALDI mass spectrometry. The purified protein fragment contains an N-terminal GS dipeptide remaining from the thrombin cleavage site.

The ^{15}N-labeled sample used for the heteronuclear NOE (hNOE), *J*-modulated HSQC, ^{15}N NOESY-HSQC, and ^{15}N HSQC-TOCSY experiments contains a five-residue C-terminal extension with the sequence GIHRD that originates from the pGEX vector. This C-terminal extension is added to an unstructured portion of the gate peptide and causes chemical shift perturbations only of resonances from residues nearby in sequence, indicating that the presence of these amino acids does not cause structural changes.

For the disulfide-linked construct, the amino acid triplet CGG was incorporated into the gate peptide sequence immediately following the thrombin cleavage site, and a GGC amino acid triplet was added immediately preceding the stop codon. The protein was expressed, purified, and cleaved in a manner similar to that of the wild-type contruct and air-oxidized at pH 8.0. Formation of the intramolecular disulfide bond was monitored by C18 HPLC and chemical shift perturbations in HSQC spectra.

NMR Spectroscopy. NMR spectra were acquired on a Brüker DMX-500 MHz spectrometer equipped with a ^{1}H, ^{15}N, ^{13}C triple-resonance, triple-axis gradient probe. The ^{15}N HSQC-TOCSY and ^{13}C HSQC-NOESY data were acquired on a Brüker DMX-750 MHz spectrometer similarly equipped. All spectra were acquired at 16 °C on approximately 1 mM samples buffered at pH 6.5 with 25 mM potassium phosphate. Samples also contained 1 mM sodium azide, 1 mM PMSF, and 1 mM EDTA. NMRPipe (*17*) was used to process all data; peak picking and intensity measurement were accomplished using PIPP (*18*). Spectra were typically apodized with 72° phase-shifted sine-bell-squared functions and forward linear predicted in indirectly acquired dimensions to twice the acquired size prior to zero filling and Fourier transformation. Spectra from which peak intensities were determined were apodized with 90° phase-shifted sine-bell-squared functions. Assignment was accomplished using homonuclear TOCSY (τ_m = 30 and 70 ms), ^{15}N HSQC-TOCSY (τ_m = 75.5 ms), HNHB, CT-HNCA, CT-HN(CO)-CA, and HCCH-TOCSY (τ_m = 26 ms) spectra (*19*−*21*). Because of resonance overlap, the backbone resonances of Lys 1480, Lys 1481, Lys 1482, and Lys 1519 could not be sequentially assigned. Unassigned side chain resonances include primarily lysines and prolines in unstructured regions.

Heteronuclear NOEs measured as described previously (*22*, *23*) are reported as the ratio of peak intensity in the presence and absence of NOE mixing. $J_{HN\alpha}$ coupling constants were measured using a *J*-modulated HSQC pulse sequence as described previously (*23*, *24*). Seven spectra with τ_2 delays of 10, 20, 30, 40, 50, 60, and 70 ms were collected, and coupling constants were fitted from the peak intensities using NONLIN (*25*). C_α chemical shifts are reported relative to the random coil chemical shifts (*26*).

Structure Determination. NOE distance constraints were obtained from homonuclear NOESY (two constraints), ^{15}N NOESY-HSQC (203 constraints), ^{13}C NOESY-HSQC (69 constraints), and ^{13}C HSQC-NOESY (125 constraints) spectra all collected with mixing times of 120 ms except for the homonuclear NOESY spectrum which was collected with a 200 ms mixing time. Peak intensities of unambiguously assigned NOEs were classified as strong, medium, weak, or very weak; 15 NOEs for which intensities could not be accurately determined because of resonance overlap were arbitrarily classified as very weak. Strong, medium, weak, and very weak NOEs were assigned distance constraints of 1.8−2.85, 1.8−3.75, 1.8−4.5, and 1.8−5.5 Å, respectively. R^{-6} averaging was used for degenerate protons. Side chain swapping was used for non-stereospecifically assigned protons (*27*). ϕ dihedral angles were constrained to $-60 \pm 30°$ for residues with $J_{HN\alpha}$ values of >5 Hz. χ_1 dihedrals were restrained to ±30° of the observed rotamer determined from analysis of HNHB spectra in conjunction with intraresidue NOE data.

The three-dimensional structure of the folded region of the gate peptide was determined with the program XPLOR (*28*) using a hybrid distance geometry-restrained molecular dynamics protocol (*23*, *29*) in combination with experimental distance and dihedral constraints. Only intraresidue and sequential NOE connectivities are observed for residues outside the structured region, and consequently, the structure determination was limited to residues Phe 1483−Lys 1511. From 25 starting structures, a family of 12 structures that contained no NOE violations greater than 0.3 Å and no dihedral violations greater than 3° was obtained (Table 1). The 10 lowest-energy structures were retained for further analysis.

Substituted Cysteine Mutagenesis. Mutations were introduced into the 2128 bp *Eco*RV DNA fragment, excised from the rat brain type IIa sodium channel α-subunit (*30*, *31*), in

Table 1: Structural Statistics for the Sodium Channel Inactivation Gate

total no. of distance constraints	399
intraresidue	210
sequential ($\|i - j\| = 1$)	98
intermediate ($1 < \|i - j\| \leq 4$)	79
long-range ($\|i - j\| > 4$)	12
total no. of dihedral constraints	
ϕ	10
χ_1	5
rms deviations from experimental constraints	
distance constraints (Å)	0.022 ± 0.003
dihedral constraints (deg)	0.15 ± 0.20
rms deviations from ideal geometry	
covalent bonds (Å)	0.0033 ± 0.0003
covalent angles (deg)	0.58 ± 0.03
impropers (deg)	0.28 ± 0.01
average pairwise atomic rms differences[a]	
backbone N, C_α, and C atoms (Å)	0.65 ± 0.14
all heavy atoms (Å)	1.8 ± 0.2

[a] Residues Phe 1489−Lys 1503.

mp18RV as described previously (*32*) and confirmed by DNA sequencing. The mutant cassette was subcloned into pCDM8rIIa containing the remainder of the rIIa sodium channel gene and the T7 bacteriophage promoter for in vitro RNA transcription. RNA was transcribed and injected into *Xenopus* oocytes for channel expression as described previously (*12*). The sodium channel β1-subunit was coexpressed with the α-subunit mutants. The vitelline layer was removed before patch clamp recording of macroscopic currents from cell-attached or excised inside-out patches using an extracellular (pipet) solution containing 115.0 mM NaCl, 2.5 mM KCl, 1.8 mM $CaCl_2$, 10 mM EGTA, and 10 mM HEPES (pH 7.4) and a cytoplasmic (bath) solution containing 10 mM NaCl, 140 mM KCl, 1 mM $MgCl_2$, 10 mM EGTA, and 10 mM HEPES (pH 7.4) at room temperature.

Sodium current traces were recorded during depolarizations to −30 mV (I1488C and M1490C) or −20 mV (F1489C and T1491C) from a holding potential of −140 mV before and after exposure of the cytoplasmic surface to [2-(trimethylammonium)ethyl]methanethiosulfonate bromide (MTSET; Toronto Research Chemicals, North York, Canada). MTSET was prepared every 2 h as a 2.5 mM stock solution, stored on ice, and diluted to the final concentration in a bath solution immediately prior to application. MTSET at 20 mM (I1488C) or 40 nM (F1489C, M1490C, and T1491C) was applied by exposing the cytoplasmic surface of the patch to the outflow of a tube containing this solution. Reaction with MTSET occurred within the dead time of manual mixing for F1489C, M1490C, and T1491C. The recordings in the presence of MTSET were normalized so that the activation time courses match in the absence and presence of MTSET to adjust for the slower activation observed after removal of inactivation (*33*).

RESULTS AND DISCUSSION

Structured Region of the Inactivation Gate Peptide. The isolated 53-residue inactivation domain contains a stably structured region as indicated by dynamics measurements, chemical shift data, and *J* coupling constants (Figure 1). Although the termini are mobile and flexible with negative hNOE values, residues in the central portion of the inactivation gate peptide have positive hNOEs indicative of stable structure. The structured region of the gate peptide includes the hydrophobic IFM motif and extends C-terminally to Ser 1506, which is required for modulation of inactivation by protein kinase C (*34*). The folded region is flanked N-terminally by Gly 1484 and Gly 1485 and C-terminally by a proline-rich sequence, both of which have been proposed to function as hinges for the gate (*35*). $J_{HN\alpha}$ coupling constants and C_α chemical shift perturbations are consistent with the hNOE data (Figure 1) and indicate the presence of a helical stretch within the folded region. Although positive hNOE values indicate the structured region extends from Asp 1487 to Ser 1506, the backbone conformation of the gate peptide is well-determined only from residue Phe 1489 to Lys 1503; constraint information for structured residues outside this range is insufficient to yield a defined conformation (Figure 2A). In addition to a well-defined backbone conformation, a subset of side chains also show well-defined conformations.

In the native sodium channel, the ends of the III−IV linker are thought to be tethered near each other (*1*, *2*). Comparison of HSQC spectra of the wild-type gate peptide and a construct in which the termini have been linked via a disulfide bond reveals only minor chemical shift perturbations of resonances near the peptide termini. Although many residues that show negative hNOEs in the wild-type construct have hNOEs near zero in the disulfide-linked construct, no additional residues with positive hNOEs are observed in the disulfide-linked construct (data not shown). These observations indicate that linking the peptide ends does reduce the mobility of the termini, but does not result in the formation of any additional structure. The glycine- and proline-rich regions flanking the folded core are unstructured in both peptide constructs, consistent with their proposed role as hinges in the intact channel (*35*).

Structural Implications for the Hinged Lid Mechanism. The backbone of the inactivation gate forms an α-helix capped at its N terminus by a turn structure, with the hydrophobic IFM motif immediately N-terminal to this turn (Figure 2B). Ser 1506, the target of PKC, is at the extreme C-terminal end of the helix. This location, distal from the IFM motif, suggests that modulation of inactivation by PKC phosphorylation occurs by an indirect mechanism. Met 1490 in the IFM motif packs against the helix, forming a hydrophobic cluster that includes Gln 1494, Tyr 1497, Tyr 1498, and Met 1501. This cluster of amino acids is well-defined by NOE correlations between Met 1501 and both tyrosine rings, long-range NOEs between Met 1490 and Tyr 1498, and NOE connectivities between the two aromatic rings. The location of Met 1490 in this hydrophobic cluster indicates that Met 1490 likely serves primarily an indirect role in inactivation, helping define and stabilize the structure of the inactivation gate. Additional roles for amino acids in this cluster cannot, however, be ruled out. Tyr 1497 and Tyr 1498 have been implicated in coupling activation and inactivation, and channel variants in which these tyrosines are replaced by glutamine show altered kinetics of both activation and inactivation (*12*, *36*). Although packed against one another, these residues are still partially solvent-exposed and may interact with other parts of the channel.

While Met 1490 is packed against the helix and likely serves an indirect, structural role in inactivation, the two other

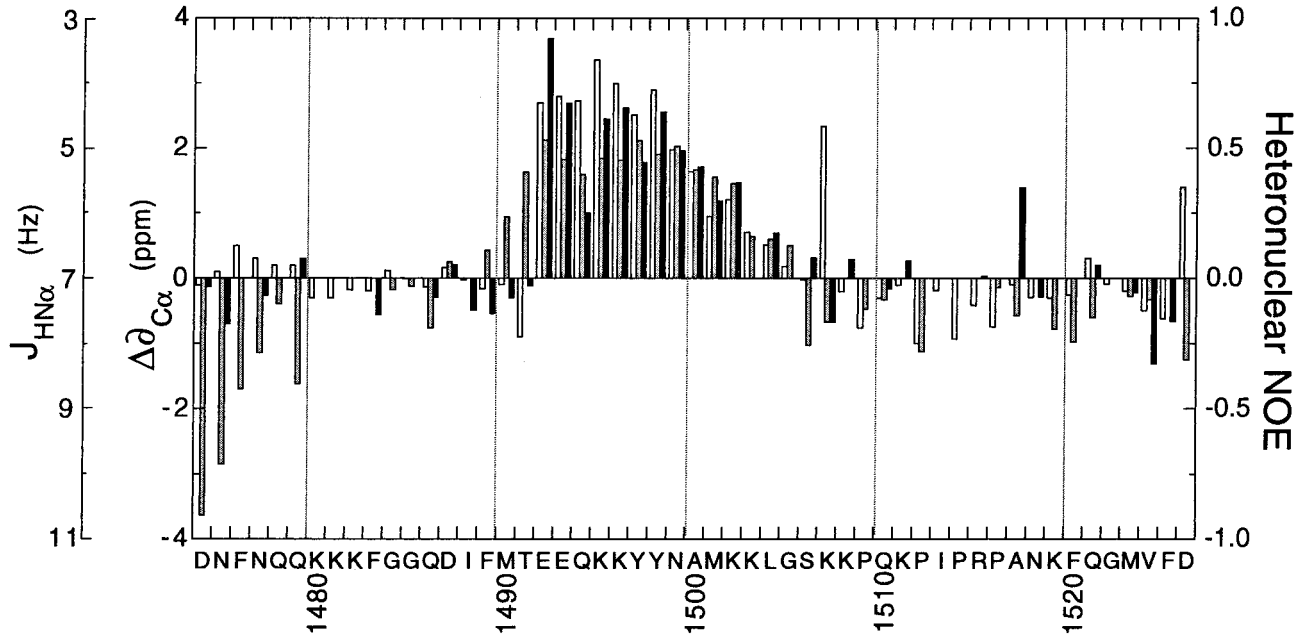

FIGURE 1: NMR parameters for the inactivation gate peptide. Heteronuclear NOEs (gray bars), $J_{HN\alpha}$ coupling constants (black bars), and C_α chemical shifts (white bars) identify a stably structured region of the inactivation gate peptide.

members of the hydrophobic triad are solvent-exposed and available to interact directly with the rest of the channel. NOE evidence indicates that Phe 1489 and Ile 1488 do not pack into the tyrosine-methionine cluster, but are located on the surface facing away from Met 1490. No NOEs are observed between the side chains of Met 1490 and either Ile 1488 or Phe 1489, indicating that these residues, although adjacent in sequence, are not spatially proximate. NOEs are observed, however, between the side chains of Phe 1489 and Thr 1491 and between the side chains of Ile 1488 and Phe 1489, demonstrating that these three residues are close in space. Neither Ile 1488 nor Phe 1489 has well-defined side chain rotamers, but instead, they appear to be solvent-exposed and flexible. The disposition of Ile 1488 or Phe 1489 is surprising given the proximity of a hydrophobic cluster with which these side chains could interact, suggesting that the solvent accessibility of these residues is functionally required for inactivation.

Electrophysiological measurements of wild-type and mutant intact channel variants also suggest functional differences between the role of Met 1490 and that of Ile 1488 and Phe 1489 in inactivation. Single-site mutations changing the hydrophobic triad residues to glutamine indicate that Phe 1489 is the most critical residue for inactivation (*13*). Inactivation is almost completely abrogated in the F1489Q mutant, while substantially smaller defects are observed for I1488Q and M1490Q mutants. Interestingly, while incorporating a phenylalanine at position 1488 partially suppresses the effect of the F1489Q mutation, a F1489Q/M1490F double mutant shows increased sustained currents relative to the single F1489Q mutation (*12*). The determined structure provides an explanation for this observation; side chains at positions 1488 and 1489 are both solvent-exposed, allowing the phenylalanine in the F1489Q/I1488F double mutant to partially function in place of the wild-type phenylalanine. In contrast, the side chain at position 1490 is packed away from the putative interaction surface, preventing a phenylalanine at this position from substituting for the wild-type Phe 1489.

Given the drastic effect of Phe 1489 mutations and the accessibility of this residue in the gate structure, the surface of the inactivation gate containing Phe 1489 likely serves as the "latch" which mediates interaction between the inactivation gate and the channel pore. Several studies have implicated the hydrophobic character of this putative interaction surface as being critical to inactivation. A series of mutants at position 1489 shows a strong correlation between side chain hydrophobicity and the ability to inactivate (*12*); introduction of a hydrophilic Ag^+ moiety effectively abrogates inactivation in a F1489C variant, and addition of charged groups to this cysteine via methanethiosulfonate (MTS) reagents dramatically reduces the rate and extent of inactivation (*16*).

IFMT Latch Motif. While the putative interaction surface revealed by the structure of the gate peptide does contain a substantial hydrophobic patch arising from the Ile 1488 and Phe 1489 side chains, this surface also has significant contributions from polar (Thr 1491) and charged (Glu 1492 and Glu 1493) side chains and from the peptide backbone (Figure 3A). The prominence of hydrophilic character on this surface suggests that the interface between the inactivation domain and the channel pore may be mediated by interactions more complex than simple hydrophobicity. The role of Glu 1492 and Glu 1493 in inactivation is not yet well defined. These negatively charged residues likely help stabilize the gate structure through favorable interaction with the helix macrodipole, but mutations which neutralize these negative charges do not strongly affect inactivation (*11*). Examination of less conservative mutations or the effects of thiol modification at these positions will be necessary to ascertain any possible role for these residues in inactivation. In contrast, physiological evidence indicates that Thr 1491 is a critical residue for inactivation. The point mutation T1491M, which increases the hydrophobic character of the surface, has been linked to paramyotonia congenita, an autosomal dominant disorder characterized by abnormal muscle membrane excitability leading to muscle stiffness (*37*). Elec-

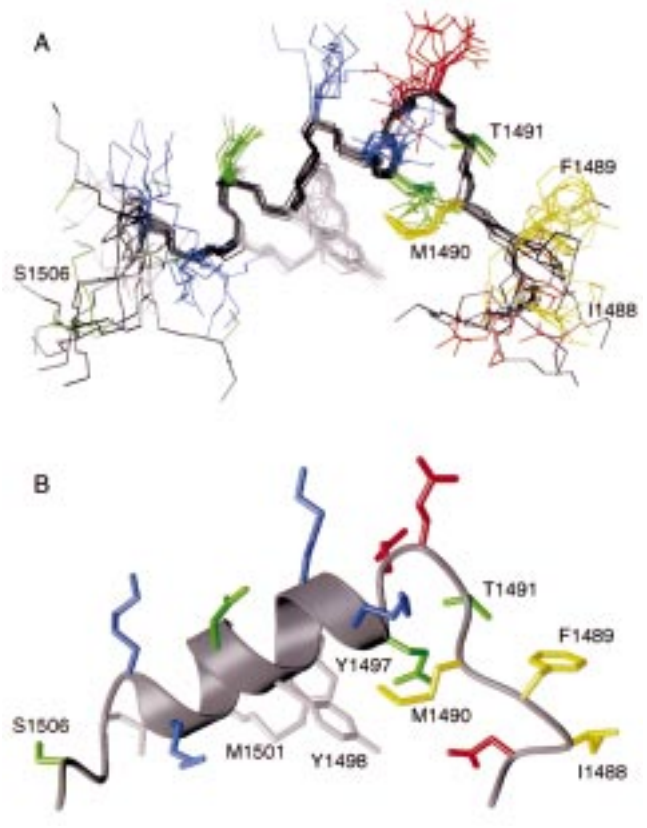

FIGURE 2: Structure of the sodium channel inactivation gate peptide. The backbone is gray, and side chains comprising the hydrophobic IFM motif are yellow. Other side chains are colored by amino acid property: nonpolar (white), polar (green), negatively charged (blue), and positively charged (red). (A) Superposition of the 10 lowest-energy structures of the inactivation gate peptide. C_α atoms of residues Phe 1489−Lys 1503 are superimposed. (B) Ribbon representation of the average refined structure of the inactivation gate. The structure was subjected to 500 steps of Powell minimization to remove bad contacts and geometries resulting from averaging. Figures were created using Spock (J. A. Christopher, Department of Biochemistry, Texas A&M University, College Station, TX), Molscript (*45*), and Raster3D (*46*).

trophysiological measurements have demonstrated that the defect is in fast inactivation (*12*, *38*, *39*).

Thiol modification of single cysteine variants of the intact channel with MTS ethyltrimethylammonium (MTSET) also indicates that the interaction between the gate and its receptor site on the pore requires more than hydrophobic side chains (Figure 4). In excised inside-out patches from *Xenopus* oocytes, mutants I1488C, F1489C, and M1490C have nearly normal time courses of activation and inactivation, while inactivation of the T1491C mutant is markedly slowed. Reaction of the bulky, charged ethyltrimethylammonium group with the I1488C mutant has only a small effect on inactivation. In contrast, addition of MTSET to the F1489C, M1490C, or T1491C variants completely blocks inactivation (Figure 4) (*16*). Comparison of the putative interaction surface colored by either hydrophobicity or sensitivity to thiol modification reveals a disparity (compare panels A and B in Figure 3). Ile 1488, which contributes to the surface hydrophobicity, is not critically important for inactivation. In contrast, inactivation is highly sensitive to modification of the polar residue Thr 1491. It is unclear whether Thr 1491 serves primarily a structural role or directly participates in the gate−pore interaction. While Thr 1491 is solvent-exposed and adjacent to Phe 1489, its side chain hydroxyl is within hydrogen-bonding distance of the amide protons of Glu 1493 and Gln 1494, suggesting that Thr 1491 caps the α-helix. Mutations which remove the hydrogen bond acceptor and increase hydrophobicity (T1491M and T1491V) lead to reduced extents of inactivation (*12*). The hydrogen bond acceptor is retained and surface hydrophobicity decreased in a T1491D mutant, but this variant shows very similar inactivation defects (*12*). Additional structural and functional analysis of mutants at position 1491 will be required to dissect the relative contributions of Thr 1491 to structural integrity versus the gate−pore interaction surface. Nevertheless, the results of these cysteine-scanning mutagenesis experiments strongly support the structural data which define an interactive surface on the inactivation gate peptide that contains Ile 1488, Phe 1489, and Thr 1491 and is held in place by hydrophobic interactions of Met 1490.

Structural Studies of Ion Channels. High-resolution structural information for channels has been sparse, and models for the structural basis of channel gating have been generally based on extensive analysis of primary sequence patterns, mutagenesis data, and effects of toxins. Recently, however, the structures of two different regions of voltage-gated potassium channels have been reported. The X-ray crystal structure of the potassium channel from *Streptomyces lividans* has provided the first high-resolution view of a voltage-gated channel pore, and has provided insights into the mechanisms of ion conduction and selectivity (*40*). The sequences of sodium and potassium channels are homologous in the pore region, making it likely that the structures of the channel pores are also highly similar. In contrast, the inactivation domains of sodium and potassium channels do not share significant sequence homology, and comparison of the present sodium channel inactivation gate structure with voltage-gated potassium channel inactivation particles indicates that they differ structurally as well. The *Shaker* inactivation domain does not adopt a well-defined structure in solution (*41*, *42*). Two other potassium channel inactivation domains, RAW3-IP and RCK4 (*43*), show unique solution structures that differ substantially from the sodium channel gate. The sodium channel gate and the RAW3-IP structure have completely different backbone folds; the RCK4 inactivation particle shows general similarities to the sodium channel inactivation gate in that both contain helical regions and N-terminal turns, but the detailed structures of the two particles differ significantly. Although the inactivation domains of potassium and sodium channels are functional homologues (*44*), they mediate inactivation via distinct sequences, structures, and detailed mechanisms.

Conclusion. The structure presented here represents the first high-resolution data available for voltage-gated sodium channels. The domain III−IV linker in isolation contains a stably structured subdomain comprised of an α-helix capped by an N-terminal turn structure. The structured subdomain contains residues functionally implicated in mediating and regulating inactivation and is flanked by regions proposed to serve as hinge regions for the inactivation gate. Phe 1489 and Met 1490 of the hydrophobic IFM motif are critical for inactivation, with the phenylalanine positioned to directly interact with the pore, and the methionine likely playing an indirect but crucial structural role, positioning the interaction

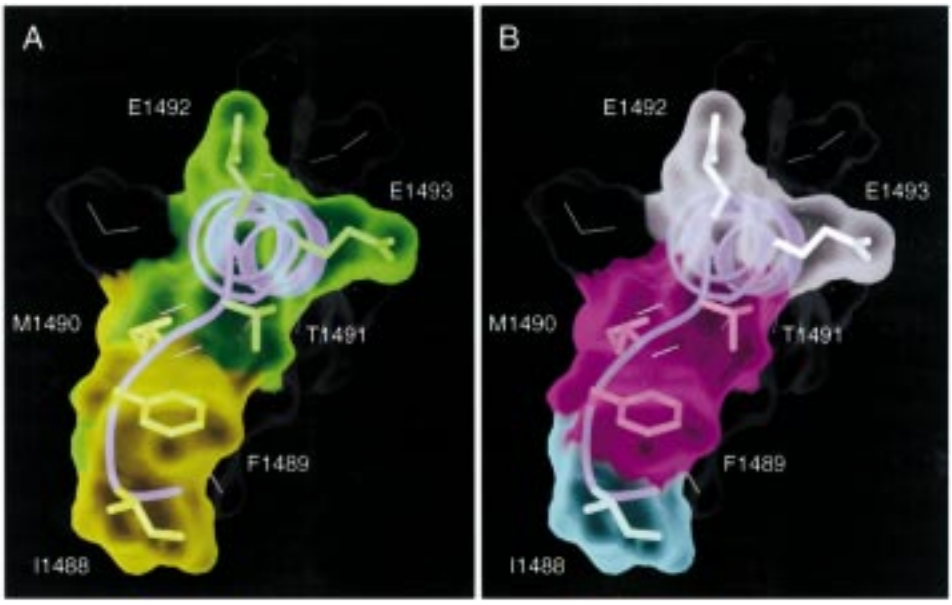

FIGURE 3: Putative interaction surface of the sodium channel inactivation gate. The view is approximately along the helical axis. (A) Hydrophobic side chains and associated molecular surface are yellow; polar side chains and surface are green. (B) Surface and side chains are colored by sensitivity to thiol modification: insensitive (cyan), sensitive (fuchsia), and unknown (white).

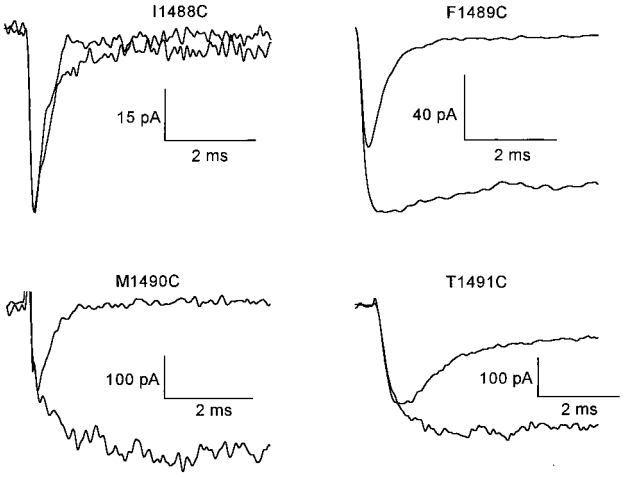

FIGURE 4: Effect of sulfhydryl modification of cysteine residues substituted in the IFMT motif. Sodium current traces were recorded from cell-attached (I1488C, no MTSET) or excised inside-out patches from *Xenopus* oocytes expressing the mutant sodium channels during depolarizations to −30 mV (I1488C and M1490C) or −20 mV (F1489C and T1491C) from a holding potential of −140 mV before and after exposure of the cytoplasmic surface to 20 mM MTSET for I1488C, 40 nM MTSET for F1489C (*16*), 40 nM MTSET for M1490C, and 40 nM MTSET for T1491C. The traces with impaired inactivation were obtained in the presence of MTSET.

surface of the gate for binding to the channel pore. While Ile 1488 may contribute to the general hydrophobic environment of the interaction surface, its role in the gate−pore interface appears to be peripheral. In contrast, both structural and functional analysis of Thr 1491 indicate that this residue is an integral member of the latch motif, suggesting that while the hydrophobic IFM was originally proposed to serve as the gate latch, the tetrad IFMT may be a more accurate designation of the latch motif. Our results provide a structural view of fast inactivation of sodium channels by this highly conserved motif.

ACKNOWLEDGMENT

We thank Dr. Ponni Rajagopal for her assistance with NMR experiments and Dr. Anthony Fodor for critical review of the manuscript.

REFERENCES

1. Catterall, W. A. (1992) *Physiol. Rev. 72*, S15−S48.
2. Fozzard, H. A., and Hanck, D. A. (1996) *Physiol. Rev. 76*, 887−926.
3. Keating, M. T., and Sanguinetti, M. C. (1996) *Curr. Opin. Genet. Dev. 6*, 326−333.
4. Marban, E., Yamagishi, T., and Tomaselli, G. F. (1998) *J. Physiol. 508*, 647−657.
5. Armstrong, C. M., and Bezanilla, F. (1977) *J. Gen. Physiol. 58*, 567−590.
6. Cannon, S. C. (1996) *Annu. Rev. Neurosci. 19*, 141−164.
7. Cantrell, A. R., Ma, J. Y., Scheuer, T., and Catterall, W. A. (1996) *Neuron 16*, 1019−1026.
8. Vassilev, P. M., Scheuer, T., and Catterall, W. A. (1988) *Science 241*, 1658−1661.
9. Vassilev, P., Scheuer, T., and Catterall, W. A. (1989) *Proc. Natl. Acad. Sci. U.S.A. 86*, 8147−8151.
10. Stühmer, W., Conti, F., Suzuki, H., Wang, X., Noda, M., Yahagi, N., Kubo, H., and Numa, S. (1989) *Nature 339*, 597−603.
11. Patton, D. E., West, J. W., Catterall, W. A., and Goldin, A. L. (1992) *Proc. Natl. Acad. Sci. U.S.A. 89*, 10905−10909.
12. Kellenberger, S., West, J. W., Scheuer, T., and Catterall, W. A. (1997) *J. Gen. Physiol. 109*, 589−605.
13. West, J. W., Patton, D. E., Scheuer, T., Wang, Y., Goldin, A. L., and Catterall, W. A. (1992) *Proc. Natl. Acad. Sci. U.S.A. 89*, 10910−10914.
14. Eaholtz, G., Scheuer, T., and Catterall, W. A. (1994) *Neuron 12*, 1041−1048.
15. Eaholtz, G., Zagotta, W. N., and Catterall, W. A. (1998) *J. Gen. Physiol. 111*, 75−82.
16. Kellenberger, S., Scheuer, T., and Catterall, W. A. (1996) *J. Biol. Chem. 271*, 30971−30979.
17. Delaglio, F., Grzesiek, S., Vuister, G. W., Zhu, G., Pfeifer, J., and Bax, A. (1995) *J. Biomol. NMR 6*, 277−293.
18. Garrett, D. S., Powers, R., Gronenborn, A. M., and Clore, G. M. (1991) *J. Magn. Reson. 95*, 214−220.

19. Archer, S. J., Ikura, M., Torchia, D. A., and Bax, A. (1991) *J. Magn. Reson. 95*, 636−641.
20. Grzesiek, S., and Bax, A. (1992) *J. Magn. Reson. 96*, 432−440.
21. Kay, L. E., Xu, G.-Y., Singer, A. U., Muhandiram, D. R., and Forman-Kay, J. D. (1993) *J. Magn. Reson. B 101*, 333−337.
22. Farrow, N. A., Muhandiram, R., Singer, A. U., Pascal, S. M., Kay, C. M., Gish, G., Shoelson, S. E., Pawson, T., Forman-Kay, J. D., and Kay, L. E. (1994) *Biochemistry 33*, 5894−6003.
23. Jones, B. E., Rajagopal, P., and Klevit, R. E. (1997) *Protein Sci. 6*, 2107−2119.
24. Billeter, M., Neri, D., Otting, G., Qian, Y. Q., and Wüthrich, K. (1992) *J. Biomol. NMR 2*, 257−274.
25. Johnson, M. L., Correia, J. J., Yphantis, D. A., and Halvorson, H. R. (1981) *Biophys. J. 36*, 575−588.
26. Wishart, D. S., Bigam, C. G., Holm, A., Hodges, R. S., and Sykes, B. D. (1995) *J. Biomol. NMR 5*, 67−81.
27. Folmer, R. H. A., Hilbers, C. W., Konings, R. N. H., and Nilges, M. (1997) *J. Biomol. NMR 9*, 245−258.
28. Brünger, A. T. (1987) *X-PLOR Version 3.1: A system for X-ray crystallography and NMR*, Yale University Press, New Haven, CT.
29. Nilges, M., Clore, G. M., and Gronenborn, A. M. (1988) *FEBS Lett. 229*, 317−324.
30. Auld, V. J., Goldin, A. L., Krafte, D. S., Marshall, J., Dunn, J. M., Catterall, W. A., Lester, H. A., Davidson, N., and Dunn, R. J. (1988) *Neuron 1*, 449−461.
31. Auld, V. J., Goldin, A. L., Krafte, D. S., Catterall, W. A., Lester, H. A., Davidson, N., and Dunn, R. J. (1990) *Proc. Natl. Acad. Sci. U.S.A. 87*, 323−327.
32. Rogers, J. C., Qu, Y., Tanada, T. N., Scheuer, T., and Catterall, W. A. (1996) *J. Biol. Chem. 271*, 15950−15962.
33. Gonoi, T., and Hille, B. (1987) *J. Gen. Physiol. 89*, 253−274.
34. West, J. W., Numann, R., Murphy, B. J., Scheuer, T., and Catterall, W. A. (1991) *Science 254*, 866−868.
35. Kellenberger, S., West, J. W., Catterall, W. A., and Scheuer, T. (1997) *J. Gen. Physiol. 109*, 607−617.
36. O'Leary, M. E., Chen, L.-Q., Kallen, R. G., and Horn, R. (1995) *J. Gen. Physiol. 106*, 641−658.
37. McClatchey, A. I., Van den Bergh, P., Pericak-Vance, M. A., Raskind, W., Verellen, C., McKenna-Yasek, D., Rao, K., Haines, J. L., Bird, T., Brown, R. H., Jr., and Gusell, J. F. (1992) *Cell 68*, 769−774.
38. Hayward, L. J., Brown, R. H., Jr., and Cannon, S. C. (1996) *J. Gen. Physiol. 107*, 559−576.
39. Hayward, L. J., Brown, R. H., Jr., and Cannon, S. C. (1997) *Biophys. J. 72*, 1204−1219.
40. Doyle, D. A., Cabral, J. M., Pfuetzner, R. A., Kuo, A., Gulbis, J. M., Cohen, S. L., Chait, B. T., and MacKinnon, R. (1998) *Science 280*, 69−81.
41. Fernandez-Ballester, G., Gavilanes, F., Albar, J. P., Criado, M., Ferragut, J. A., and Gonzalez-Ros, J. M. (1995) *Biophys. J. 68*, 858−865.
42. Schott, M. K., Antz, C., Frank, R., Ruppersberg, J. P., and Kalbitzer, H. R. (1998) *Eur. Biophys. J. 27*, 99−104.
43. Antz, C., Geyer, M., Fakler, B., Schott, M. K., Guy, H. R., Frank, R., Ruppersberg, J. P., and Kalbitzer, H. R. (1997) *Nature 385*, 272−275.
44. Patton, D. E., West, J. W., Catterall, W. A., and Goldin, A. L. (1993) *Neuron 11*, 967−974.
45. Kraulis, P. J. (1991) *J. Appl. Crystallogr. 24*, 946−950.
46. Merritt, E. J., and Bacon, D. J. (1997) *Methods Enzymol. 277*, 505−524.

BI9823380